OPEN ACCESS
IOP Publishing
Plasma Physics and Controlled Fusion
Plasma Phys. Control. Fusion **61** (2019) 045003 (12pp)
https://doi.org/10.1088/1361-6587/aaf9c3

ELM-induced cold pulse propagation in ASDEX Upgrade

E Trier[1], E Wolfrum[1], M Willensdorfer[1], Q Yu[1], M Hoelzl[1], F Orain[1], F Ryter[1], C Angioni[1], M Bernert[1], M G Dunne[1], S S Denk[1,2], J C Fuchs[1], R Fischer[1], P Hennequin[3], B Kurzan[1], F Mink[1,2], A Mlynek[1], T Odstrčil[1,2], P A Schneider[1], U Stroth[1,2], G Tardini[1], B Vanovac[4], the ASDEX Upgrade team and EUROfusion MST1 Team[5]

[1] Max Planck Institute for Plasma Physics, D-85748 Garching, Germany
[2] Physik-Department E28, Technische Universität München, D-85748 Garching, Germany
[3] Laboratoire de Physique des Plasmas, Ecole Polytechnique, CNRS, F-91128 Palaiseau Cedex, France
[4] DIFFER—Dutch Institute for Fundamental Energy Research, Eindhoven, The Netherlands

E-mail: elisee.trier@ipp.mpg.de

Received 3 August 2018, revised 6 December 2018
Accepted for publication 19 December 2018
Published 15 February 2019

Abstract

In ASDEX Upgrade, the propagation of cold pulses induced by type-I edge localized modes (ELMs) is studied using electron cyclotron emission measurements, in a dataset of plasmas with moderate triangularity. It is found that the edge safety factor or the plasma current are the main determining parameters for the inward penetration of the T_e perturbations. With increasing plasma current the ELM penetration is more shallow in spite of the stronger ELMs. Estimates of the heat pulse diffusivity show that the corresponding transport is too large to be representative of the inter-ELM phase. Ergodization of the plasma edge during ELMs is a possible explanation for the observed properties of the cold pulse propagation, which is qualitatively consistent with non-linear magneto-hydro-dynamic simulations.

Keywords: ELMs, MHD instabilities, stochastic field, magnetic islands, cold pulse

(Some figures may appear in colour only in the online journal)

1. Introduction

Understanding the electron heat transport in tokamaks is necessary to predict the performance of future fusion reactors. While it has been widely studied in the core [1, 2], less attention has been given to its characterization in the edge-core coupling region, say $0.7 \lesssim \rho_{pol} \lesssim 0.95$ (where ρ_{pol} is the normalized poloidal radius). This zone connects the pedestal, where the kinetic profiles evolution is constrained by magnetohydrodynamic (MHD) stability, with the confinement zone governed by turbulent processes and profiles stiffness [3]. It has been shown that the edge region can have a strong impact on the overall confinement [4, 5]. In this region, transport should influence the spatial extension of the area affected by the edge localized modes (ELMs), and could then have an impact on ELM-induced energy losses [6–8].

In this article, the inward propagation of electron temperature T_e perturbations (or 'cold pulses') induced by type-I ELMs is analyzed, in ASDEX Upgrade. At a typical ELM frequency of 100 Hz and a pulse propagation time of 1–3 ms, a non-negligible 10%–30% time fraction of an H-mode phase can be covered by these events. Moreover, the ELM loss power corresponds to 15%–40% of the power crossing the separatrix in ASDEX Upgrade [8], which is a significant contribution to the total electron heat losses. Thus, useful information for the modeling of the global confinement in H-mode, or the ELM cycle can be obtained from the analysis of the propagation of T_e perturbations.

Similar approaches have long been used with outward propagating sawteeth-induced heat pulses, following initial studies in the ORMAK tokamak [9]. Later, similar investigations

[5] See author list in H Meyer *et al* 2017 *Nucl. Fusion* **57** 102014.

Original content from this work may be used under the terms of the Creative Commons Attribution 3.0 licence. Any further distribution of this work must maintain attribution to the author(s) and the title of the work, journal citation and DOI.

 © 2019 Max-Planck-Institut fur Plasmaphysik Printed in the UK

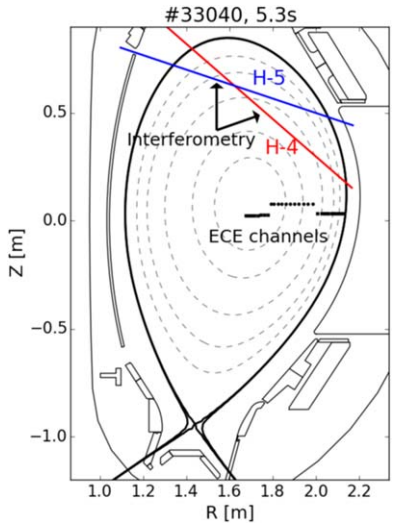

Figure 1. Location of ECE measurements, in a typical example (shot #33040). The interferometry lines of sight 'H-4' and 'H-5' are also shown.

on TFTR [10, 11] led to the conclusion that a transient increase of heat diffusivity during the sawtooth crash—possibly due to MHD activity—was occurring. In this study, we will discuss the possibility of such a temporary increase of transport subsequent to an ELM in the region where the cold pulses propagate.

The article is organized as follows: in section 2, the database of ASDEX Upgrade plasmas used in this study is described; a quantification of the inward penetration of an ELM-induced T_e perturbation is also defined. In section 3, the sensitivity of the ELM penetration to various plasma parameters is presented, showing a dominant effect of the plasma current or the edge safety factor. Section 4 deals with transport: the possible contribution of the source terms in the energy equation is discussed, and an estimate of the heat pulse diffusivity is given, leading to the conclusion that the transport is too large to be representative of the inter-ELM phase. In section 5, a possible explanation is presented, related with the ergodization of the plasma edge during ELMs, and qualitatively consistent with non-linear MHD simulations.

2. Methodology

2.1. Dataset of ASDEX Upgrade H-mode plasmas

In ASDEX Upgrade (major radius $R = 1.65$ m, minor radius $a \simeq 0.5$ m, elongation $k \simeq 1.6$), the electron temperature is measured by a 60 channels electron cyclotron emission (ECE) heterodyne radiometer, which detects the second harmonic extraordinary mode at an on-axis toroidal magnetic field B_t of -2.5 T [12, 13]. The system consists of 24 channels with a spatial resolution of 12 mm, and 36 channels with a resolution of 5 mm at the edge. The measurements are located slightly above the midplane (see figure 1). The sampling rate is 1 MHz; in this study the data is down-sampled to 8 kHz. A 1 ms-median filter is systematically applied to each channel individually; note that this results in an averaging over the faster T_e fluctuations, such as those potentially caused by the motion of 3D structures rotating at the plasma perpendicular velocity in a given measurement volume.

Table 1. Parameter range in the database, with median values in brackets: plasma current I_p, toroidal magnetic field B_t, edge safety factor q_{95}, auxiliary heating power P_{aux}, average triangularity δ, ellipticity k, deuterium fueling rate Γ_0, electron temperature and density measured by Thomson scattering at $\rho_{\text{pol}} = 0.8$, and ELM frequency f_{ELM} (average number of ELMs per second).

Parameter	Unit	Min–Max (Median)
I_p	(MA)	0.8–1.15 (1.0)
$\lvert B_t \rvert$	(T)	2.45–2.68 (2.48)
q_{95}	—	3.5–5.3 (4.4)
P_{aux}	(MW)	2.6–13.9 (8.1)
δ	—	0.21–0.28 (0.24)
k	—	1.60–1.74 (1.64)
Γ_0	($\times 10^{22}$ s^{-1})	0.0–2.8 (0.97)
$n_e(0.8)$	($\times 10^{19}$ m^{-3})	3.5–7.3 (6.4)
$T_e(0.8)$	(keV)	0.7–1.4 (1.0)
f_{ELM}	(Hz)	33–183 (97)

Table 2. Pearson correlation coefficient between parameters in the database: plasma current, magnetic field, triangularity, auxiliary heating, deuterium fueling rate and electron density at $\rho_{\text{pol}} = 0.8$. Absolute values greater than 0.7 are highlighted.

	q_{95}	δ	P_{aux}	Γ_0	$n_e(0.8)$
q_{95}	(1.0)				
δ	0.26	(1.0)			
P_{aux}	**−0.72**	0.23	(1.0)		
Γ_0	−0.54	−0.04	**0.57**	(1.0)	
$n_e(0.8)$	**−0.73**	−0.04	**0.58**	**0.69**	(1.0)

The penetration of ELM-induced cold pulses, subsequent to the initial electron temperature crash, is analyzed in a database of 46 ASDEX Upgrade stationary H-mode deuterium plasmas (time-window ranging from 0.5 to 1.85 s) with type-I ELMs. No magnetic perturbations are applied during the considered time-windows.

In table 1, the range of some relevant global and local parameters is displayed. The necessity of having ECE measurements at the plasma edge limits the variations of electron density, which remains below the cut-off limit, and of the magnetic field which lies in the interval $B_t = -2.57 \pm 0.12$ T. Consequently, the edge safety factor q_{95} mainly depends on the plasma current. The average triangularity δ has been kept to moderate values $0.21 \leqslant \delta \leqslant 0.28$, in order to avoid too strong ELMs that could introduce uncertainty in the analysis due to their impact on plasma equilibrium (this effect is discussed in section 3.3).

The correlations between engineering parameters (plasma current I_p, toroidal magnetic field B_t, triangularity δ, auxiliary heating power P_{aux}, deuterium fueling rate Γ_0)—plus the edge electron density n_e at a normalized poloidal radius $\rho_{\text{pol}} = 0.8$—are shown in table 2. A rough correlation between I_p (or q_{95}) and n_e is difficult to avoid, since the

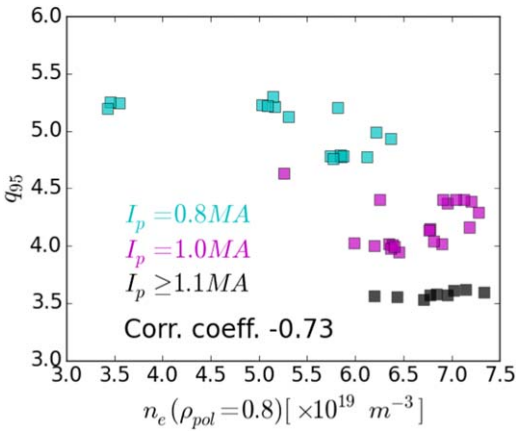

Figure 2. Considered plasmas in the (n_e (0.8), q_{95}) plane, where the time-averaged electron density is measured by Thomson scattering.

'natural' density is proportional to the plasma current [14]. This is shown in figure 2 for this dataset. For this reason, the effect of electron density and edge safety factor are jointly considered in section 3. The correlation between the auxiliary heating P_{aux} and q_{95} is also significant.

2.2. Quantifying the ELM penetration

In this study, the drop in edge T_e due to an ELM is considered as a boundary perturbation for the inner plasma, occurring at the outer limit of the region of interest. The latter is chosen in the pedestal top region $\rho_{\text{pol}} = 0.95$. The T_e perturbation propagates inwards due to electron heat transport, experiencing a time-delay and a decay in amplitude. This results in the lowering of the correlation between $T_e(\rho_{\text{pol}} = 0.95, t)$ and T_e measured by radially separated more inner ECE channels $T_e(\rho_{\text{pol}} \leqslant 0.95, t)$.

A parameter designed as *ELM penetration radius* is introduced to quantify the penetration depth of the ELM-induced cold pulses. It is defined here as the normalized poloidal radius for which the Pearson correlation coefficient between $T_e(\rho_{\text{pol}}, t)$ and $T_e(0.95, t)$ drops to a value of 0.5.

The Pearson correlation coefficient for two random variables X and Y is here computed from their discrete time-series (X_i, Y_i):

$$\text{corr}(X, Y) = \frac{\sum_i (X_i - \bar{X})(Y_i - \bar{Y})}{\sqrt{\sum_i (X_i - \bar{X})^2} \times \sqrt{\sum_i (Y_i - \bar{Y})^2}} \in [-1, 1]$$

where $\bar{X}$ is the mean value of X. This coefficient quantifies the linear correlation between two variables. An absolute value of 1 indicates a perfect fit. Although this is necessarily arbitrary, it will be considered in this article that the correlation is strong for absolute values above 0.7, and weak below 0.5.

A smaller ELM penetration radius means a deeper penetration, and a larger, more radially extended region perturbed by the ELMs. For each stationary plasma from the dataset, radial profiles of T_e correlation between ρ_{pol} and $\rho_{\text{pol}} = 0.95$ are calculated by averaging over a series of ten 200 ms long time-windows. Similar results than those presented below have also been obtained with a time-window inversely proportional to the ELM frequency (rather than fixed at 200 ms, thus containing an approximately constant number of ELMs). Another remark is that the method used here is not affected by the presence of smaller ELMs that may occur between type-I ELMs, because the correlation is more sensitive to values with a large deviation from the mean.

3. Results: sensitivity of the ELM penetration

In this section, the sensitivity of the ELM penetration radius on plasma parameters is analyzed. In particular, the safety factor/plasma current, the edge electron density and pressure, the ELM strength, and possible ELM-induced radial displacements of the bulk plasma are considered.

3.1. Safety factor profile or plasma current

In figure 3, the electron temperature perturbation $T_e(\rho_{\text{pol}}, t) - \langle T_e \rangle(\rho_{\text{pol}})$ (where the brackets refer to the mean value in the considered time-interval) induced by the ELMs is represented by color maps in the (ρ_{pol}, t) plane for 3 discharges with different plasma current ($I_p = 0.8$, 1.0, and 1.1 MA). The ELM-affected region is more extended at lower I_p (subfigure (a)).

The influence of the plasma current and safety factor is confirmed in figure 4(a), where the profiles of T_e correlation with $\rho_{\text{pol}} = 0.95$ are displayed for each plasma from the dataset. A color code is used to distinguish the various plasma currents ($I_p = 0.8$, 1.0, or 1.10–1.15 MA), and shows that different behaviors are observed. A similar trend is visible in figure 4(b), where the radial averaged profiles of ELM-induced T_e perturbations (normalized to the maximum value, for each ELM) are presented.

In figure 5(a), the resulting ELM penetration radius is plotted against the edge safety factor q_{95}: there is a strong correlation of -0.84 (or 0.87 with the plasma current) between these two parameters. The error bars of the correlation coefficients are evaluated by varying the experimental points within the error bars in a large number of draws (10 000) and calculating the standard deviation of the resulting set of correlation values. Note that this strong correlation between the ELM penetration radius and q_{95} is not due to the use of ρ_{pol} as a radial coordinate. Indeed, this correlation is even larger if the normalized toroidal radius ρ_{tor} is used in the definition of the ELM penetration radius (i.e. considering the T_e correlation drop from a reference channel at$\rho_{\text{tor}} = 0.89$, whose average position corresponds to $\rho_{\text{pol}} = 0.95$): in this case the correlation between the corresponding ELM penetration radius and q_{95} reaches -0.89. Thus, the safety factor or the plasma current should be playing a role in determining the electron heat transport after an ELM crash in this near-edge region. This observation is completed in the remaining part of this section by considering other possible parameters that could also have influenced the ELM penetration, but are in fact of secondary influence: the edge electron density/pressure, the ELM strength, and possible ELM-induced radial displacements of the plasma.

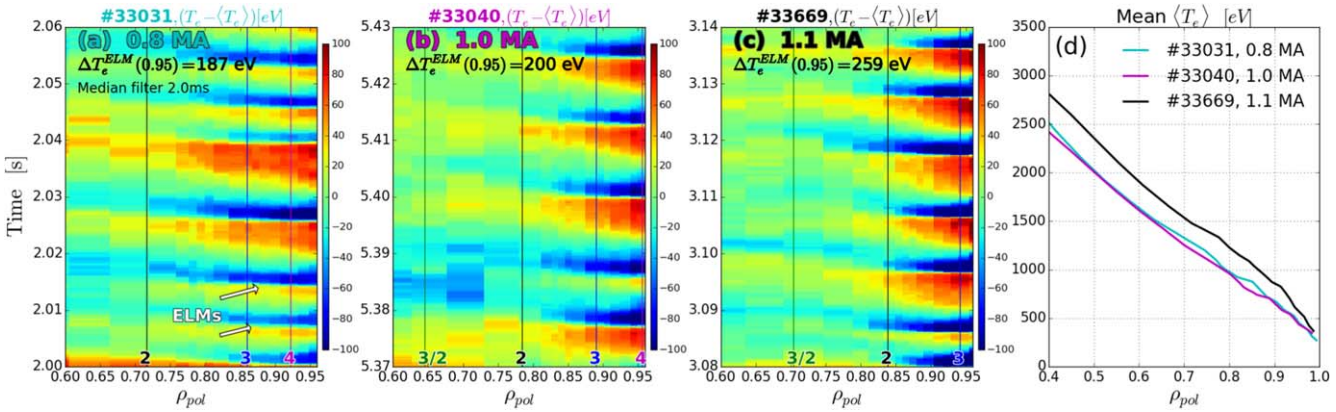

Figure 3. (a)–(c) Color maps of the T_e perturbation ($T_e(\rho_{\rm pol}, t) - \langle T_e\rangle(\rho_{\rm pol})$) for 3 shots with $I_p = 0.8$, 1.0, and 1.1 MA, as a function of time and the time-averaged $\rho_{\rm pol}$. The positions of low-order rational surfaces are indicated by the vertical lines. (d) Mean $\langle T_e\rangle$ radial profiles.

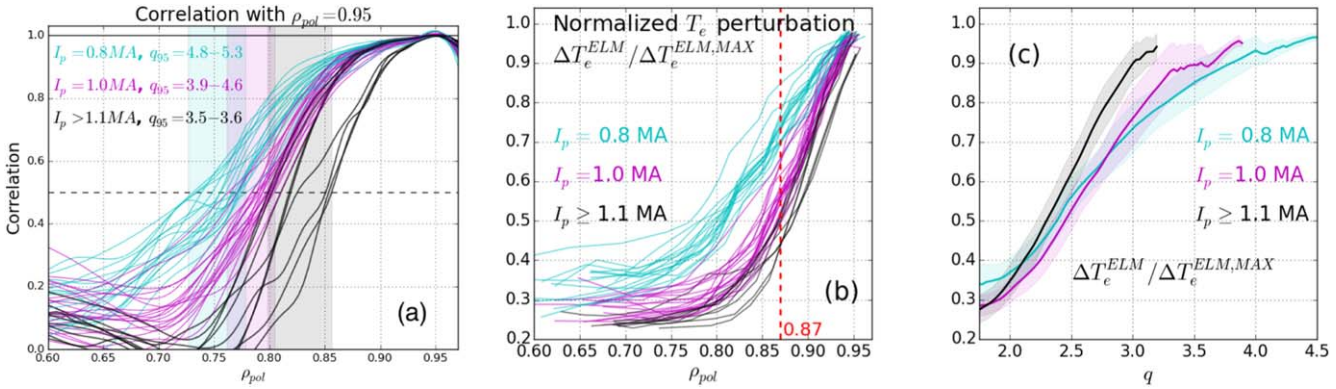

Figure 4. (a) Radial profiles of correlation with the channel at $\rho_{\rm pol} = 0.95$ for all discharges. Ranges of ELM penetration radius are indicated by the shaded areas. (b) Radial average profiles of the ELM-induced electron temperature perturbation $\Delta T_e^{\rm ELM}$, normalized for each ELM by the maximum perturbation $\Delta T_e^{\rm ELM,MAX}$. (c) Similar to (b), $\Delta T_e^{\rm ELM}/\Delta T_e^{\rm ELM,MAX}$ as a function of the safety factor, averaged for each group of different I_p (the influence of q is discussed in the following sections).

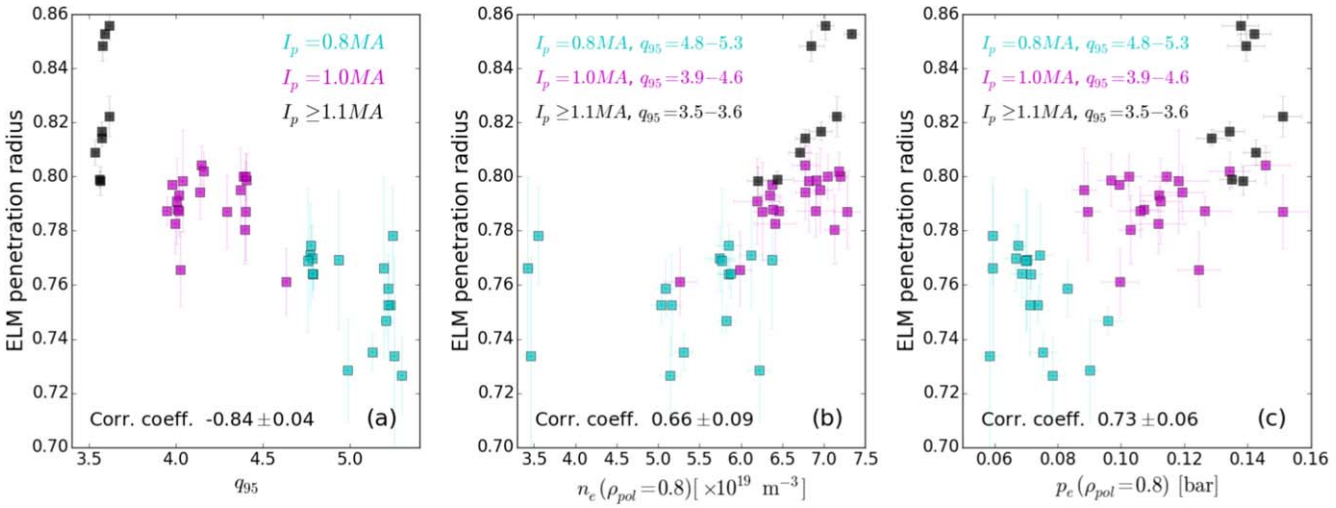

Figure 5. (a) ELM penetration radius as a function of the edge safety factor q_{95}, (b) the edge electron density $n_e(0.8)$ or (c) the edge electron pressure $p_e(0.8)$. The correlation coefficient between the plotted quantities is indicated.

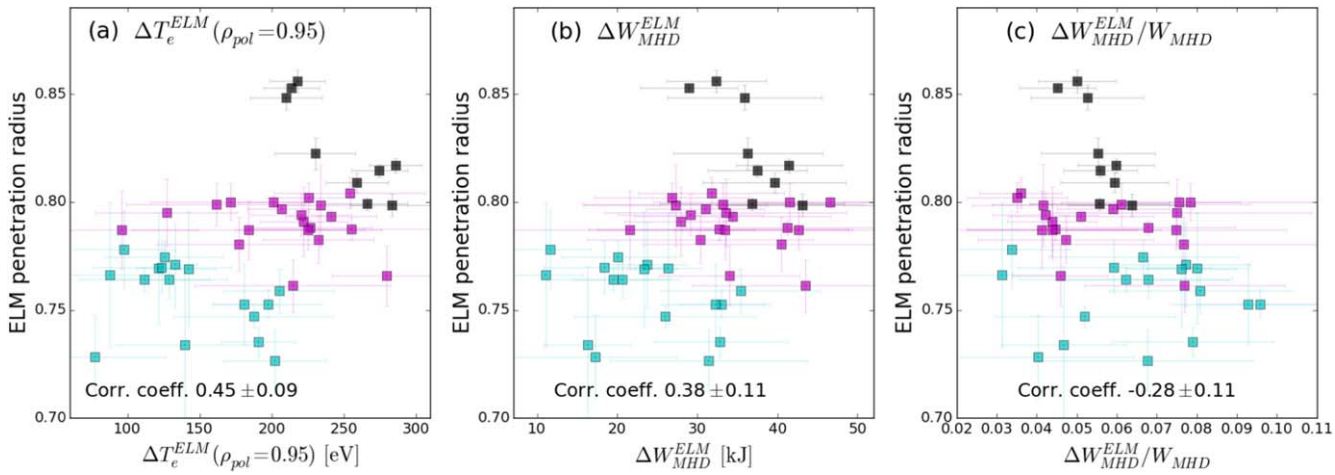

Figure 6. ELM penetration radius for all plasma discharges, as a function of the median values of: (a) the ELM-induced T_e drop at $\rho_{\mathrm{pol}} = 0.95$, noted $\Delta T_e^{\mathrm{ELM}}$, (b) the drop of plasma stored energy $\Delta W_{\mathrm{MHD}}^{\mathrm{ELM}}$ and (c) the relative drop $\Delta W_{\mathrm{MHD}}^{\mathrm{ELM}}/W_{\mathrm{MHD}}$. The more shallow penetration in spite of the stronger ELM strength in subfigures (a) and (b) can be noticed.

3.2. Edge density and pressure

As shown in figure 2, the edge density is correlated with the plasma current in this dataset (and the edge safety factor). It is then expected that the ELM penetration radius is also correlated with the edge density. This is shown in figure 5(b): such a correlation exists, but is weaker in comparison with the influence of the safety factor in figure 5(a). The absolute correlation with the ELM penetration radius are 0.66 for the density and 0.84 for the q_{95}. Similarly, the correlation between the penetration radius and the edge pressure $p_e(0.8)$ is 0.73. However, in this dataset $p_e(0.8)$ and q_{95} are strongly correlated (correlation coefficient value is -0.87), because of the increase of the pedestal top pressure with the plasma current [15]. The correlation of $p_e(0.8)$ with the ELM penetration radius should therefore be a consequence of the stronger correlation between the ELM penetration radius and q_{95} or I_p. The influence of the edge electron density or pressure on ELM penetration cannot be excluded, but the observed hierarchy in correlations indicates a subdominant influence in comparison with the safety factor or plasma current.

3.3. ELM 'strength'

The ELM strength would appear as a natural candidate to explain the differences in ELM-induced cold pulse penetration. It can be evaluated by several quantities, which are considered in figure 6: the median value of the ELM-induced T_e drop at $\rho_{\mathrm{pol}} = 0.95$, noted $\Delta T_e^{\mathrm{ELM}}$ (subfigure (a)), the ELM-induced drop of plasma stored energy $\Delta W_{\mathrm{MHD}}^{\mathrm{ELM}}$ (subfigure (b)) or its relative variation $\Delta W_{\mathrm{MHD}}^{\mathrm{ELM}}/W_{\mathrm{MHD}}$ (subfigure (c)). As pointed by the low correlation between these parameters and the ELM penetration radius, the ELM strength is not the main explanation for the cold pulse penetration. An interesting observation in subfigures (a) and (b) is that at larger plasma current, the ELM penetration is more shallow in spite of the generally stronger absolute drop in plasma energy and edge T_e.

3.4. ELM-induced plasma motion

During an ELM, a fraction of the plasma current [16] and stored energy is expelled from the pedestal region. This can lead to a temporary inaccuracy of the externally applied vertical magnetic field used for maintaining the equilibrium, and to radial or vertical displacements of the bulk plasma. Passive structures surrounding the plasma, and inner control coils with a time response of about 2 ms are mitigating these effects.

The radial location of ECE measurements, which depends on the value of the magnetic field, remains approximately constant during an ELM within typically 2–3 mm. Since they are mostly located on the low field side and close to the equatorial plane (see figure 1), a radial inward displacement of the bulk plasma should in principle be seen as a drop in T_e, proportional to the electron temperature gradient and the amplitude of the radial jump. Such a perturbation should also affect simultaneously all the channels on the low field side, that are located in a region with non-zero T_e gradient. The corresponding artificial T_e perturbation caused by the vertical bulk motion should be smaller, because this displacement would be quasi-tangent to the magnetic surfaces at the ECE measurements location.

Unfortunately, obtaining an estimate of the ELM-induced motion of the bulk plasma is made difficult by the currents induced temporarily by the ELMs in the surrounding structures, which perturbate the magnetic measurements.

Nevertheless, in this dataset the effect of the ELM-induced bulk plasma motion on T_e measurements should be too small to explain the observed cold pulse propagation, for the following reasons:

– The ELM-induced jump of $R_{\mathrm{med}} = (R_{\mathrm{in}} + R_{\mathrm{out}})/2$, noted $\Delta R_{\mathrm{med}}^{\mathrm{ELM}}$ and where R_{in} and R_{out} are the separatrix inner and outer major radius, can be used as a proxy to estimate ELM-induced bulk plasma motion. This quantity is estimated from an equilibrium reconstruction based on magnetic measurements. Even if its accuracy

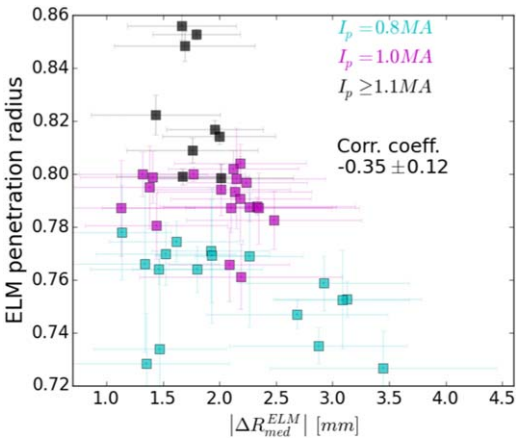

Figure 7. ELM penetration radius as a function of the median value of the ELM-induced (inward) jump of $R_{\rm med}$, $|\Delta R_{\rm med}^{\rm ELM}|$.

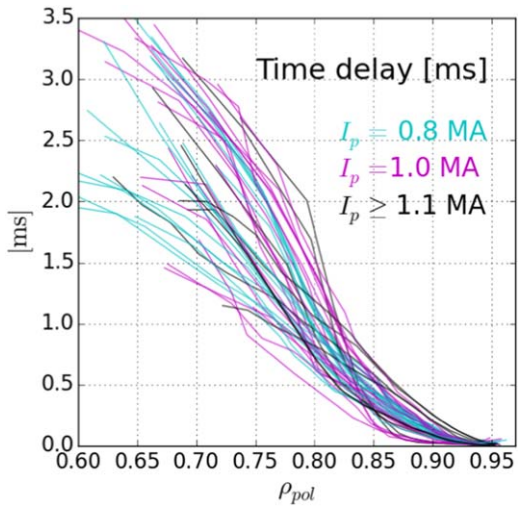

Figure 8. Radial profiles of the average cold pulse time-delay (defined in the text) for all the considered plasmas. Note that the unclear dependence of the time-delay on the plasma current is briefly discussed at the end of section 4.

is questionable because of the currents in the structures mentioned above, a reasonable assumption would be that $\Delta R_{\rm med}^{\rm ELM}$ is increasing with the 'real' bulk plasma motion. As shown in figure 7, $\Delta R_{\rm med}^{\rm ELM} < 3.5$ mm, and the correlation between the ELM-induced radial jump $\Delta R_{\rm med}^{\rm ELM}$ and the ELM penetration radius is weak. Moreover, the corresponding 'artificial' T_e perturbation is of the order $\Delta T_e^{\rm motion} \sim \Delta R_{\rm med}^{\rm ELM} \times a \times {\rm d}T_e/{\rm d}\rho_{\rm pol}$, where a is the plasma minor radius. Evaluating the radial derivative of the electron temperature profile at $\rho_{\rm pol} = 0.8$, the corresponding $\Delta T_e^{\rm motion}$ would lie in the range 5–25 eV for this dataset, which is smaller than the ELM-induced T_e perturbation ($70 < \Delta T_e^{\rm ELM} < 285$ eV). For this dataset, the ratio $\Delta T_e^{\rm motion}/\Delta T_e^{\rm ELM}$ is always smaller than 20%, with mean and median values of 7%.

– The signature of an inward motion of the bulk plasma should be a drop of T_e affecting simultaneously the channels on the low field side, depending on the local T_e gradient. However, it is possible to track the temporal evolution of the ELM-induced cold pulses. This has been done by evaluating, for each ELM and ECE channel, the first moment of the negative part of the time-derivative $(\partial T_e/\partial t)^-$ in a time-windows $[t_{\rm ELM} - 1.5\,{\rm ms},\ t_{\rm ELM} + 3\,{\rm ms}]$, as long as the ELM-induced T_e drop remains above 20% of its maximum value. Thus, the inwards propagation of the T_e crash is tracked, and the time-delay is defined using as reference the minimum crash time obtained for a given ELM. The median (over every ELMs of a shot) time-delay profiles are shown in figure 8. They differ from the 'flat' time-delay profiles that would have been caused by an ELM-induced bulk plasma motion.

Table 3. Correlation with the ELM penetration radius, sorted by the decreasing absolute value: edge safety factor q_{95}, electron pressure, density and β at $\rho_{\rm pol} = 0.8$ (noted $p_e(0.8)$, $n_e(0.8)$, $\beta_e(0.8)$), ELM frequency $f_{\rm ELM}$, auxiliary heating power $P_{\rm aux}$, magnetic shear s, average triangularity δ, electron temperature with its absolute and logarithmic gradient at $\rho_{\rm pol} = 0.8$ ($T_e(0.8)$, $\nabla T_e(0.8)$, $\nabla T_e/T_e(0.8)$), median value of ELM-induced crash of T_e at $\rho_{\rm pol} = 0.95$ ($\Delta T_e^{\rm ELM}$) or the plasma stored energy ($\Delta W_{\rm MHD}^{\rm ELM}$), energy confinement time τ_E, dimensionless parameters $\rho_s^*(0.8)$ and $\nu_{ei}^*(0.8)$ and electron to ion temperature ratio at $\rho_{\rm pol} = 0.8$.

Corr. with ELM penetration radius	
q_{95}	**−0.843 ± 0.045**
$p_e(0.8)$	**0.735 ± 0.058**
$n_e(0.8)$	**0.662 ± 0.087**
$\beta_e(0.8)$	**0.652 ± 0.062**
$f_{\rm ELM}$	**0.637 ± 0.073**
$P_{\rm aux}$	**0.566 ± 0.059**
$s(0.8)$	−0.514 ± 0.129
$T_e(0.8)$	0.509 ± 0.065
δ	−0.508 ± 0.070
$\lvert\nabla T_e(0.8)\rvert$	0.507 ± 0.066
$\Delta T_e^{\rm ELM}$	0.448 ± 0.090
$\rho_s^*(0.8)$	0.401 ± 0.064
$\nu_{ei}^*(0.8)$	−0.384 ± 0.081
$\Delta W_{\rm MHD}^{\rm ELM}$	0.382 ± 0.106
$\lvert\nabla T_e/T_e(0.8)\rvert$	0.367 ± 0.106
$\Delta R_{\rm med}^{\rm ELM}$	−0.348 ± 0.119
τ_E	−0.347 ± 0.091
$\Delta W_{\rm MHD}^{\rm ELM}/W_{\rm MHD}$	−0.278 ± 0.113
$T_e/T_i(0.8)$	−0.219 ± 0.124

3.5. Overview of the parameter sensitivity of the ELM penetration radius

The influence of other global (auxiliary heating $P_{\rm aux}$, triangularity δ, energy confinement time τ_E), local ($\beta_e \propto n_e\, T_e/B_t^2$, $\rho_s^* \propto \sqrt{T_e}/B_t$, $\nu_{ei}^* \propto q_{95}\, n_e\, T_e^{-2}$, T_e, ∇T_e, T_e/T_i, magnetic shear $s \simeq \rho_{\rm tor} \times \partial\ \ln\ q/\partial\rho_{\rm tor}$, all evaluated at $\rho_{\rm pol} = 0.8$), or ELM-related (ELM frequency $f_{\rm ELM}$) parameters have also been tested. Their correlation with the ELM penetration radius is summarized in table 3. The primary dependence (discussed above) is with q_{95} or I_p. Other parameters having a significant correlation with the ELM penetration radius are:

Table 4. Correlation with the dominant parameter q_{95}.

Corr. with q_{95}	
$p_e(0.8)$	**−0.871**
$n_e(0.8)$	**−0.728**
$\beta_e(0.8)$	**−0.856**
f_{ELM}	**−0.706**
P_{aux}	**−0.720**

$n_e(\rho_{\mathrm{pol}} = 0.8)$, $p_e(\rho_{\mathrm{pol}} = 0.8)$, $\beta_e(\rho_{\mathrm{pol}} = 0.8)$, f_{ELM}. However, they are also strongly correlated with the dominant parameter q_{95} (see table 4): therefore, with this dataset it is not possible to conclude whether these parameters have a direct influence on the ELM-induced cold pulse penetration. It is also interesting to note the lower correlation between the ELM penetration radius and the magnetic shear: it is therefore the safety factor rather than the magnetic shear that is playing a role. Even if the auxiliary heating power is significantly correlated with q_{95} (see table 2), the smaller correlation between P_{aux} and the ELM penetration radius shows a weaker influence of the additional heating. Parameters which are potentially influencing the regime of turbulence (ν^*, $\nabla T_e/T_e$, T_e/T_i) are weakly correlated with the ELM penetration radius. The low correlation (−0.35) with the energy confinement time τ_E can also be noted. In fact the increase of τ_E with I_p predicted by scaling laws [17] is in this dataset counterbalanced by the variety of auxiliary heating powers (the correlation between I_p and τ_E is −0.58). It appears that the link between global confinement and the propagation of ELM-induced cold pulses is not straightforward for the studied plasmas. Also, note that the conclusions given in this section are robust against slight changes in the definition of the ELM penetration radius, section 2.2: they remain valid if the correlation threshold used in this definition is varied around the chosen value of 0.5 (e.g. ±0.1).

To summarize this section, the inward propagation of the ELM-induced cold pulses is dominantly affected by the safety factor or the plasma current. Interestingly, with increasing plasma current the ELM penetration is more shallow in spite of the stronger ELMs.

4. Estimation of transport

In this section, an attempt to relate the behavior of the cold pulses to the transport properties of the near-edge region is presented. Because ELMs are strong perturbations that can affect the magnetic structure, there is no *a priori* reason to assume that, during the time-interval when the cold pulses propagate, the edge transport is stationary and representative of the inter-ELM phase. And indeed, anticipating the evaluation of the electron heat pulse diffusivity χ_e presented in this section, large values are found at the edge that are incompatible with the assumption of a time-invariant χ_e (usually done in standard methods of transport analysis). Obtaining a precise estimate of a time-varying $\chi_e(\rho, t)$, with possibly large variations occurring in a few ms, is a much more complicated inverse problem, which is outside the scope of the present—and hence, mostly qualitative discussion.

We first address the question whether the observed cold pulse propagation could be related with the source terms in the linearized electron energy transport equation. A common form of the latter, valid for small T_e perturbations, is [1] (in the absence of perturbed source of electrons):

$$\frac{3}{2} n_{e0} \frac{\partial T_{e1}}{\partial t} = -\boldsymbol{\nabla}.\mathbf{q}_1 - T_{e0}\, \boldsymbol{\nabla}.\boldsymbol{\Gamma}_1 + S_1, \tag{1}$$

where $\mathbf{q}$ and Γ are respectively the heat and particle fluxes for the electrons. The subscripts '0' and '1' respectively refer to the unperturbed and perturbed quantities. In the absence of perturbed sources of electrons, particle conservation implies that $-T_{e0}\, \boldsymbol{\nabla}.\boldsymbol{\Gamma}_1 = T_{e0}\, \partial n_{e1}/\partial t$; this term is related to the heat flux convected by particle transport. S_1 is the perturbed heat source power density: it is the sum of the perturbed parts of the ohmic power p_1^{Ohm} density, the ion to electron energy transfer p_1^{ie}, the radiated power density $-p_1^{\mathrm{rad}}$, and the auxiliary heating p_1^{aux}. Here we assume that all quantities in equation (1) only depend on the radial variable ρ_{pol} and the time.

Let us temporarily assume (in order to prove the opposite) that the evolution of the cold pulse is dominated by the source term, so that $3/2\, n_{e0}\, \partial T_{e1}/\partial t \approx S_1$. In this case, a normalization by the perturbation initial amplitude $\Delta T_e^{\mathrm{ELM,MAX}}$ and a time-integration done in the interval $[t_0,\ t_0 + \Delta t]$ (at a given ρ_{pol}, where t_0 is the ELM starting time and Δt the time taken for the perturbation to reach its peak value) gives:

$$\frac{\Delta T_e^{\mathrm{ELM}}(\rho_{\mathrm{pol}})}{\Delta T_e^{\mathrm{ELM,MAX}}} \approx \frac{2\bar{S}_1\, \Delta t}{3\, n_{e0}\, \Delta T_e^{\mathrm{ELM,MAX}}}, \tag{2}$$

where $\Delta T_e^{\mathrm{ELM}}$ and $\Delta T_e^{\mathrm{ELM,MAX}}$ are the peak perturbations reached at the considered ρ_{pol} and the maximal perturbation value reached at the plasma edge. $\bar{S}_1$ is the time average of the source term in the interval $[t_0,\ t_0 + \Delta t]$.

Equation (2) provides two tests to check whether a given source term could indeed affect the cold pulse behavior. (i) One can test if the contribution from the source is strong enough to cause the observed peak T_{e1} perturbation. (ii) As can be guessed from figure 4(b), the left-hand side of equation (2) is strongly correlated with q_{95} (for example, the correlation coefficient between q_{95} and $\Delta T_e^{\mathrm{ELM}}(\rho_{\mathrm{pol}} = 0.87)/\Delta T_e^{\mathrm{ELM,MAX}}$ is 0.90): therefore, it can be tested if this is also the case for the right-hand side of equation (2) associated with a given source term.

For the cases where it is difficult to estimate the source power density $\bar{S}_1$ it can be assumed that it is proportional to the unperturbed part: $\bar{S}_1 \approx \alpha S_0$ where $0 < \alpha < 1$ is a certain fraction.

Ohmic power—Even the unperturbed part of the ohmic power density p_0^{Ohm} is much too small to significantly impact the T_e perturbation: an upper boundary (for this dataset) of its contribution to the change in T_e at the edge is $2/3 \times p_0^{\mathrm{Ohm}}/n_{e0} < 1\ \mathrm{eV\ ms^{-1}}$, whereas the ELM-induced drop in edge T_e is in the range 70–280 eV (see figure 6(a)).

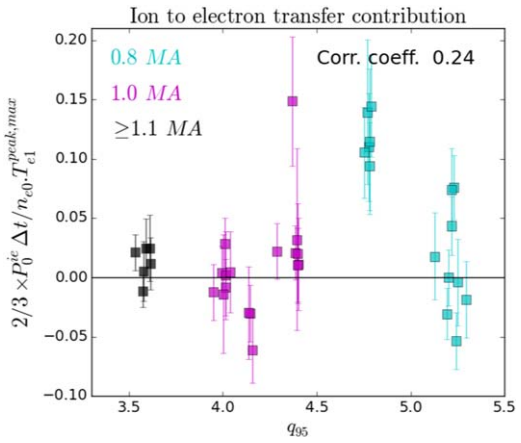

Figure 9. Contribution of the unperturbed ion to electron energy exchange to the T_e drop (see equation (2)), taking $\Delta t = 1$ ms, and evaluating the energy exchange at $\rho_{\rm pol} = 0.8$. No correlation is observed.

Ion-electron exchange—The contribution of the ion to electron energy transfer in the electron power balance equation is usually more significant than the ohmic heating. We apply the test (ii), and check if the associated right-hand side of equation (2), taking $\bar{S}_1 = p_0^{ie}$ (hence with $\alpha = 1$, which is an overestimate), is correlated with q_{95}. As shown in figure 9, this is not the case.

Radiated power—In general, the radiated power is lowered during an ELM, due to the drop of edge n_e. In ASDEX Upgrade a tomographic reconstruction from the AXUV diagnostic measurements allows an estimate of the average radiated power density. For one discharge (#33275, $I_p = 1$ MA), with a total power radiated by the plasma inside the separatrix $P^{\rm rad,tot} \simeq 3.7$ MW, the average radiated power density in the $0.7 < \rho_{\rm pol} < 0.95$ region is in the range $p_{0,\rm ref}^{\rm rad} \sim 150$–$275$ kW m^{-3}. A very rough estimate of the perturbed part of the radiated power density $p_1^{\rm rad}$ is obtained by taking as an upper boundary of the relative ELM-induced edge perturbation for the radiated power density $|p_1^{\rm rad}/p_0^{\rm rad}| \lesssim 0.5$, and evaluate $p_0^{\rm rad}$ by scaling the value for the reference plasma #33275 to an estimate of the total radiated power inside the separatrix $P^{\rm rad,tot}$: then $p_0^{\rm rad} \sim P^{\rm rad,tot}/P_{\rm ref}^{\rm rad,tot} \times p_{0,\rm ref}^{\rm rad}$. It is found that for the studied plasmas, $p_1^{\rm rad} < 225$ kW m^{-3}, and using equation (2) the associated $\Delta T_e^{\rm ELM}/\Delta T_e^{\rm ELM,MAX}$ is less than 5.5% for all the plasmas, except 3 at lower n_e for which it is less than 12%.

Auxiliary heating power—The power deposited at the edge by the ECRH and ICRH heating is negligible for the studied discharges, where the power was centrally deposited. The NBI total injected power ranges from 0 to 12 MW in this dataset. A TRANSP simulation of the plasma with $P^{\rm nbi} = 12$ MW (#32962) predicts a power density transmitted to the electrons of $\sim$400 kW m^{-3} in the $0.7 < \rho_{\rm pol} < 0.95$ region. A crude estimate of an upper boundary for the perturbed part of the absorbed NBI power density $p_1^{\rm nbi}$, in the region of interest can be obtained in the following way: the absorbed beam intensity I (particle/s) in an infinitesimal line element along the beam dx is d$I \simeq n_e \sigma I$ dx (where σ is approximately the charge-exchange cross-section for beam particle energies in the 60–90 keV range). The corresponding volumic absorbed part of the incident power $\mathscr{P}(x) = I.\langle E\rangle$ (Watts, with $\langle E\rangle$ average beam particle energy) is then $\mathrm{d}\mathscr{P}/\mathrm{d}V \simeq n_e \sigma \mathscr{P}(x)(\mathrm{d}x/\mathrm{d}V)$, where d$V$ is the infinitesimal volume element between the magnetic surfaces enclosing the line element dx. An upper boundary of d$\mathscr{P}$/dV can be obtained by taking for the incident beam power $\mathscr{P}(x)$ the total power $P^{\rm nbi}$, noting that the considered region is close to the edge. This is in an order-of-magnitude agreement with the values calculated by TRANSP for the 12 MW plasma. It follows that $(\mathrm{d}\mathscr{P}/\mathrm{d}V)_1 \sim n_{e1}/n_{e0} \times (\mathrm{d}\mathscr{P}/\mathrm{d}V)_0 \leqslant n_{e1}/n_{e0} \times (n_{e0}\sigma\, P^{\rm nbi}\mathrm{d}x/\mathrm{d}V)$. The normalized electron density drop is evaluated from the ELM-induced relative variation of the interferometer line H-5, tangential to the plasma edge (see figure 1, with a minimum $\rho_{\rm pol}$ of 0.87 typically): an upper estimate is $n_{e1}/n_{e0} < 0.15$. Taking $\sigma \simeq 2 \times 10^{20}$ m^2, and evaluating the quantities at $\rho_{\rm pol} \simeq 0.8$, it is found that $p_1^{\rm nbi} = (\mathrm{d}\mathscr{P}/\mathrm{d}V)_1 \lesssim 80$ kW m^{-3}. Using equation (2), the corresponding $\Delta T_e^{\rm ELM}/\Delta T_e^{\rm ELM,MAX}$ is for all plasmas less than 2.5%, which is too small to significantly affect the cold pulse propagation.

Therefore, the source terms should not be responsible of the observed behavior of the cold pulse propagation.

Let us now consider the term $(-\boldsymbol{\nabla}.\mathbf{q}_1 - T_{e0}\,\boldsymbol{\nabla}.\boldsymbol{\Gamma}_1)$ in equation (1), which is the sum of diffusive and convective contributions to the heat equation. The question is whether the cold pulse propagation can be described or not by stationary transport properties. We first assume that it is the case; and also ignore the $T_{e0}\boldsymbol{\nabla}.\boldsymbol{\Gamma}_1$ term (which is discussed *a posteriori*). Then, it is possible to evaluate the heat pulse diffusivity $\chi_e^{\rm hp}$, using Fourier analysis of the T_e time traces at the ELM frequency. The method is described in [1, 18], and has been widely used to analyze heat modulation experiments in ASDEX Upgrade (e.g. [2, 19]). In a slab geometry, the electron heat pulse diffusivity is calculated from the phase φ and amplitude A of the Fourier component at a perturbation frequency $f_{\rm pert}$ [2]:

$$\chi_e^{\rm amp} = \frac{3 \times 2\pi f_{\rm pert}}{4(A'/A)^2} \quad \chi_e^{\rm phase} = \frac{3 \times 2\pi f_{\rm pert}}{4\varphi'^2}$$
$$\chi_e^{\rm hp} = \sqrt{\chi_e^{\rm amp}\chi_e^{\rm phase}}, \tag{3}$$

where the prime refers to the derivative with respect to the radial variable $a_{\rm eff} \times \rho_{\rm tor}$ ($a_{\rm eff}$ is the equivalent cylindrical minor radius). The perturbation frequency is chosen as the maximum of the Fourier amplitude spectrum of the edge $T_e(t)$ in the neighboring of the ELM average frequency. The analysis, done for 4 plasmas with $I_p = 0.8$ and 1 MA, is displayed in figure 10. The ELM frequency is in the interval 88–112 Hz. For one plasma (#33031) the analysis is also applied at a frequency close to the second harmonic of $f_{\rm ELM}$, and a good agreement is found with the estimate based on the first harmonic. Very large heat pulse diffusivities $\chi_e^{\rm hp} \gtrsim 30$ m^{-2} s^{-1} are found at the plasma edge. At more

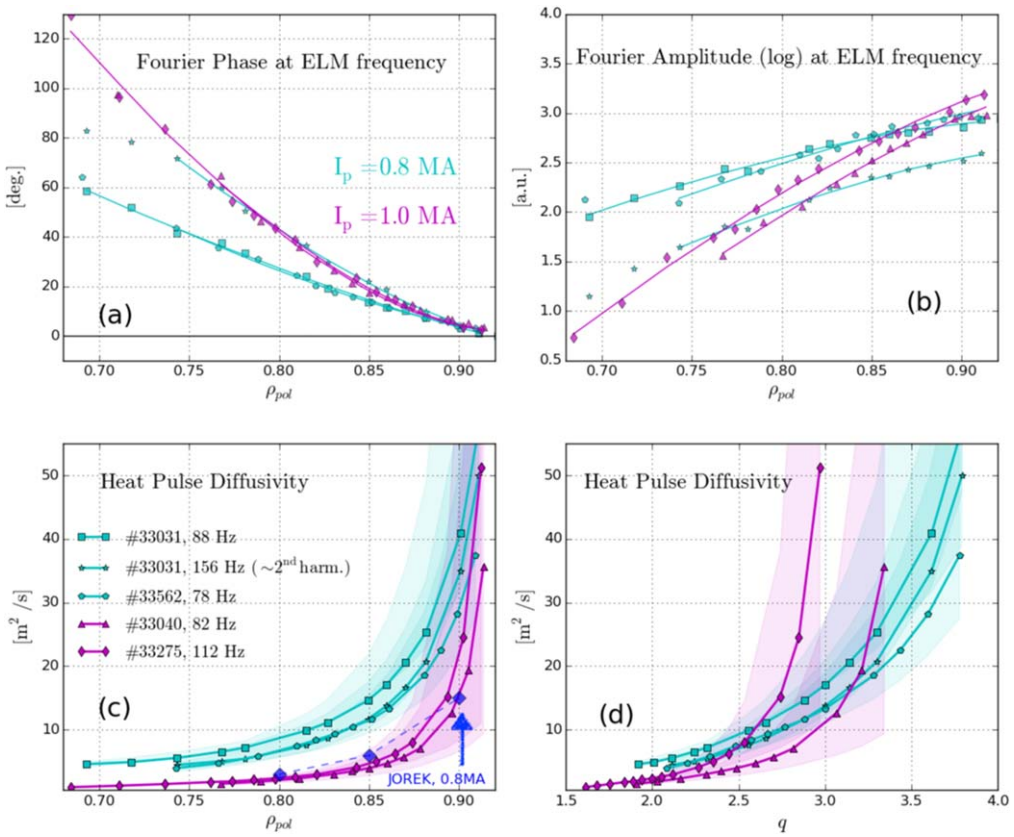

Figure 10. Estimates of the electron heat pulse diffusivity from equation $\chi_e^{\rm hp}$ (3), for 2 plasmas at $I_p = 0.8$ MA (cyan), and 2 plasmas at $I_p = 1.0$ MA (magenta). The analysis is done close to the ELM average frequency, and also close to the second harmonic for #33031. The error is evaluated by comparing $\chi_e^{\rm amp}$ and $\chi_e^{\rm phase}$. In subfigure (d), the same heat pulse diffusivity profiles are shown as a function of the safety factor. An estimate of χ_e calculated from a JOREK simulation is also shown in subfigure (c), which will be discussed in section 5.

internal radii ($\rho_{\rm pol} \sim 0.7$–0.8), $\chi_e^{\rm hp}$ is in the range 1–7 m^2 s^{-1}, which is more comparable to the typical power balance diffusivities obtained from TRANSP calculations in this region at similar plasma conditions ($\sim$1–5 m^2 s^{-1}).

The large diffusivity obtained at the edge is not compatible with stationary transport properties: a transient increase of transport is occurring when the cold pulses propagate. A contribution from the particle transport term $T_{e0}\boldsymbol{\nabla}.\boldsymbol{\Gamma}_1$ is not excluded. However the following qualitative argument shows that a similar order-of-magnitude increase of the particle diffusivity is needed to explain the large $\chi_e^{\rm hp}$ obtained in figure 10: assuming $n_{e1}/n_{e0} \simeq T_{e1}/T_{e0}$, diffusive heat and particle fluxes $\Gamma_1 = -D\nabla\ n_{e1}$, $q_1 = -n_{e0}\chi_e \nabla T_{e1}$, neglecting the source term (that cannot explain the cold pulse propagation, as shown above), and neglecting the spatial variation of the unperturbed profiles, then the equation (1) becomes a diffusion equation for T_{e1} with an apparent heat diffusivity $\bar{\chi_e} \simeq D + \chi_e$. A large value of D would therefore be required to account for the large apparent heat pulse diffusivity observed close to the edge. The other possibility involving electron heat fluxes convected by the particle transport would be the presence of a perturbed convective particle flux $\Gamma_1 = (n_e V)_1$. This cannot be excluded; but a strong convective velocity is not observed in the inter-ELM phase. Since fast and localized density measurements in the propagation region were not available, it is not possible to separate the respective diffusive and convective contributions to the total heat transport (even if a similar order-of-magnitude for χ_e and D can reasonably be expected). However, in all cases the possible explanations for the large apparent electron heat diffusivity in figure 10 (increase of electron heat diffusivity χ_e, of particle diffusivity D, or of convective particle velocity) are not compatible with the inter-ELM transport properties.

In addition, the time-variability of the transport during ELMs may be a reason why the time-delay profiles associated with the cold pulses (figure 8) do not show a clear dependence with I_p, like the amplitude profiles (figure 4(b)): the temporal (and spatial) details of the $\chi_e(\rho,\ t)$ evolution could be important in determining the cold pulse propagation.

To sum up this qualitative discussion, it was found that the source terms in the electron energy transport equation cannot explain the observed behavior of the ELM-induced cold pulses. Estimates of the heat pulse diffusivity find large values at the plasma edge, incompatible with the expectations during the inter-ELM phase. Such estimates do not explain what are the mechanisms responsible for such an increase in transport. Candidate mechanisms for describing the ELM energy losses (filaments, edge ergodization) have for example been discussed in [20]. Figure 10 suggests that these effects are also active in a part of the region where the cold pulses propagate ($0.7 < \rho_{\rm pol} < 0.95$).

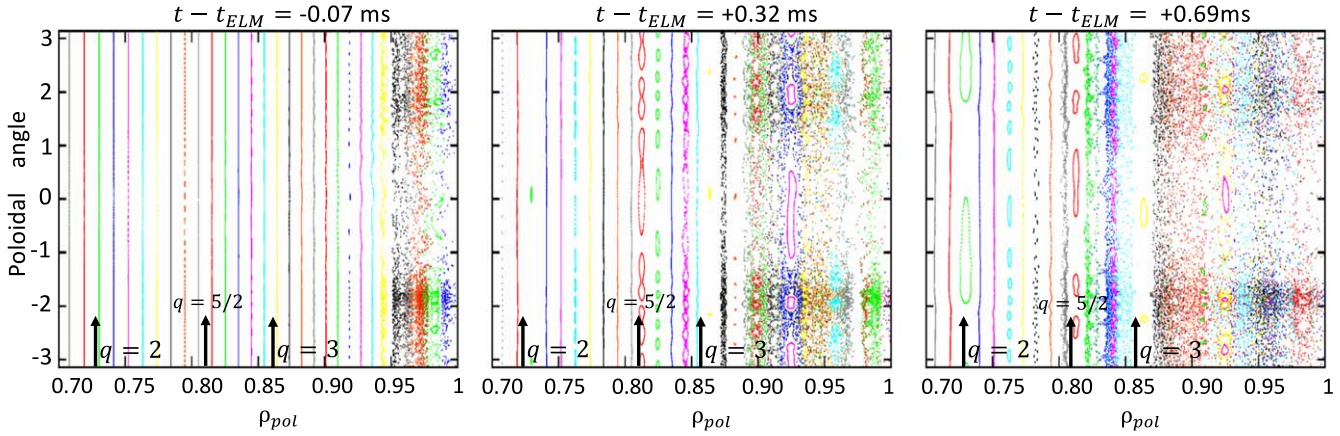

Figure 11. Poincaré plots of the magnetic field lines calculated by JOREK using as an input the kinetic profiles of shot #33616 at 7.2 s ($I_p = 0.8$ MA), and shown at three values of $t-t_{\mathrm{ELM}}$ (where t_{ELM} is the onset of the ELM crash): −0.07, 0.32, 0.69 ms. The magnetic topology is represented in the (ρ_{pol}, θ) plane. A stochastic layer at the edge, and the formation of island chains at rational surfaces (e.g. $q = 2$, $q = 5/2$) are observed.

5. Possible influence of edge ergodization

The analysis presented in section 3 has shown that the behavior of the ELM-induced cold pulses has a primary dependence on I_p or q_{95}. We cannot exclude that other parameters (edge density, pressure, ...) also play a role, but the dataset did not allow the investigation of a secondary dependence. Concerning the q_{95} or I_p influence, the cold pulse penetration should depend on the local value of some related parameter in the propagation region. Moreover, the large correlation obtained in figure 5(a) suggests that this local parameter should almost have a one-to-one correspondence with I_p and q_{95}. The local safety factor q, in particular (among other possible ones), seems to be a good candidate; whereas the local magnetic shear (see table 3) has a lower correlation with the ELM penetration radius.

One plausible hypothesis to describe the observed behavior of the ELM-induced cold pulses is related to a stochastic layer developing during the ELMs. A numerical simulation with the non-linear MHD code JOREK [21] (with realistic $E \times B$ background flows and diamagnetic effects [22]) has been run for the discharge #33616, which belongs to the $I_p = 0.8$ MA group in our dataset. The resistivity in this simulation is by a factor eight higher than in the experiment, which could lead to a slight overestimation of the stochastic layer but does not change the overall conclusions. More details regarding the simulation can be found in [23, 24]. Poincaré plots of the magnetic field lines are shown in figure 11, at three different stages of the ELM. At the edge, a region with a stochastic magnetic field develops (that will relax after 5–10 ms). Because of the strong parallel electron heat conductivity, a large radial transport is expected in the presence of stochastic field lines [25–27]. At the more external radii the field lines are connected to the divertor: as shown in figure 12 this approximately occurs outside the $q = 3$ surface. Inside $q = 3$, and up to $\rho_{\mathrm{pol}} \gtrsim 0.80$, some smaller stochastic regions are also observed (separated by magnetic islands chains and topologically unperturbed flux surfaces), but the connection length remains infinite: they are isolated from the divertor. This is thought to result from the existence of Kolmogorov–Arnold–Moser (KAM) surfaces robust against destruction, and associated with specific values of the safety factor (see e.g. [28–31]). Such surfaces can act as 'magnetic barriers' for the dispersion of field lines. In figure 12, the temporal development of the connection length after an ELM is also compared with the time-delay of the cold pulses (as plotted in figure 8, and defined in section 3.4) for the $I_p = 0.8$ MA group. It is interesting to note the change of slope occurring around $q = 3$, associated with a 'slowing down' of the cold pulses. This suggests a distinction between several regimes: (1) a fast propagation in the fully stochastic outer region connected with the divertor ($q \gtrsim 3$ in this simulation), partly controlled by the temporal development of the stochastic layer; (2) in the region where island chains are isolating the stochastic layers from each others (from $\rho_{\mathrm{pol}} = 0.80$ to $\rho_{\mathrm{pol}} \sim 0.85/q \sim 3$), a lower transport is expected, but probably still larger than the steady inter-ELM transport because of the stochasticity; (3) further inwards, the local transport properties are not perturbed by the ELM-induced changes of the magnetic structure. The dependence of these regimes onto the safety factor profile is a possible explanation for the observed strong correlation of the ELM penetration radius with q_{95} or I_p.

When we calculate the effective radial heat diffusion coefficient caused by the stochastic magnetic field according to [25, 26, 32] from the magnetic field perturbations in the JOREK simulation, values of about 3, 6, and 15 $\mathrm{m^{-2}\,s^{-1}}$ are obtained during the ELM crash at $\rho_{\mathrm{pol}} = 0.80$, 0.85 and 0.90 respectively. These values are compared with the corresponding experimental estimates at 0.8 MA (cyan curves in figure 10(c)): 7, 12, and 35 $\mathrm{m^{-2}\,s^{-1}}$. The latter are typically larger by a factor 2, which indicates a qualitative agreement. Several reasons could explain the discrepancy: the fact (discussed in section 4) that the experimental χ_e^{hp} could include some contribution from the heat transported by particle diffusion and convection, or that the simulation setup relies on an experimental equilibrium reconstruction with considerable error bars. Simulations of full ELM cycles reflecting the self-consistent evolution of the plasma into the unstable regime are expected to give a more violent ELM onset and a larger stochastisation. Such simulations are presently on their way and will be published elsewhere.

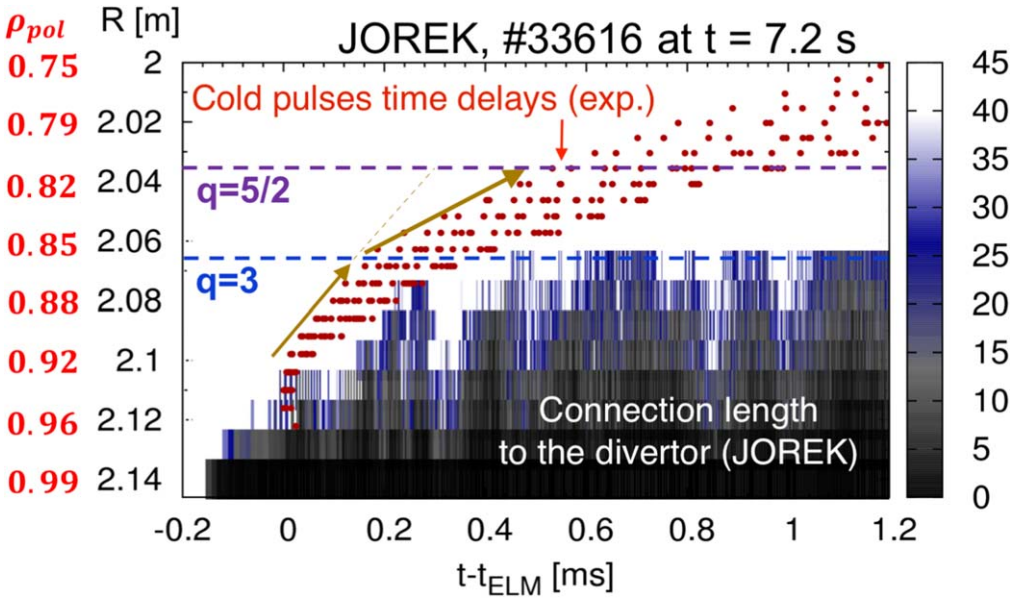

Figure 12. Time-evolution calculated by JOREK of the connection length to the divertor targets along magnetic field lines (in km), from various radial locations at the midplane. White color indicates no connection to the divertor. In red, the experimental time-delays of the cold pulses for $I_p = 0.8$ MA plasmas (as plotted in figure 8, and introduced in section 3.4) are represented.

At this point, this explanation, though consistent with observations, still remains conjectural. Additional simulations at different plasma current would be needed to check that the extent of the ELM-induced stochastic layer varies with I_p. Other effects may also play a role: for example the rotation close to a rational surface can be affected by (possibly small and ELM-seeded) magnetic islands [33], and this might cause some local shearing of the $E \times B$ velocity able to impact the transport; the role of filaments in ELM-induced power losses is also suspected [20].

Recently, in the Large Helical Device, the propagation of heat pulses has been used as a tool to study the magnetic topology, which is otherwise difficult to characterize [34, 35]. In a similar fashion, a consequence from our main hypothesis mentioned here is that, from the observed propagation of the ELM-induced cold pulses it could be possible to study how the magnetic structure is modified during the ELMs in the near-edge region.

6. Final remarks and summary

Some limits of the present analysis are:

- Because the studied plasmas have approximately the same magnetic field ($|B_t| \simeq 2.5$ T), the plasma current and the edge safety factor are strongly correlated in this dataset: therefore, it is not possible to conclude which one of these two parameters is the most important in determining the ELM penetration.
- A larger dataset would be required to study the secondary dependence of the ELM penetration, at constant I_p.
- The studied plasmas have a moderate triangularity $\delta < 0.28$. However, it is worth mentioning that a qualitatively different behavior of the cold pulse propagation is observed at larger δ: the ELM-induced T_e perturbation can be visible up to more centrally located ECE channels (this was reported in [8]), reaching typically $\rho_{\rm pol} \sim 0.5$–0.6. ELMs are stronger at large triangularity [36], and cause larger (but difficult to measure precisely) ELM-induced bulk plasma motions; for which the corresponding 'apparent' T_e variation seen by an ECE channel, proportional to the temperature gradient, may be of the order of the 'real' T_e perturbation (whereas this is not the case for the studied dataset, see section 3.3). This is why the present analysis has only focused on plasmas with $\delta < 0.28$. We note that the observation of wider ELM-affected regions at larger δ is consistent with the hypothesis of KAM surfaces (see section 5), that are in theory destroyed when the perturbation becomes sufficiently large [28].
- Due to the lack of fast and spatially resolved density measurements in the region where the cold pulses propagate, the estimates of the experimental electron heat pulse diffusivity presented in section 4 should be considered as crude. However, the observed order-of-magnitude variation allows to conclude that the transport of ELM-induced cold pulses in the near-edge region is too strong to be 'inter-ELM like'.
- The influence of stochasticity on edge transport during an ELM should be investigated in the future with MHD simulations where the plasma current is varied, and at more realistic resistivities.
- Edge ergodization alone should not be sufficient to entirely account for the cold pulse propagation. As a perturbation

propagates inwards, away from the (possibly) stochastic layer, the usual 'inter-ELM' transport is expected to become increasingly dominant. There may also be an intermediate region, where the stochasticity is weak and individual ELM-induced islands contribute to the transport of the cold pulses [27].

In summary, the propagation of cold pulses induced by type-I ELMs has been studied using ECE measurements in a dataset of 46 discharges with moderate trianguarity ($0.21 \leqslant \delta \leqslant 0.28$). It was found that the safety factor profile or the plasma current are the main determining parameters for the inward penetration of the T_e perturbations. Interestingly, with increasing plasma current the ELM penetration is more shallow in spite of the stronger ELMs. Estimates of the heat pulse diffusivity have shown that the corresponding transport is too large to be representative of the inter-ELM phase. The observed propagation could be a footprint of the ergodization of magnetic field lines occurring during ELMs.

Acknowledgments

We would like to thank Emiliano Fable, Karl Lackner, Patrick McCarthy and Wolfgang Treutterer for helpful discussions.

This work has been carried out within the framework of the EUROfusion Consortium and has received funding from the Euratom research and training programme 2014–2018 and 2019–2020 under grant agreement No. 633053. The views and opinions expressed herein do not necessarily reflect those of the European Commission.

ORCID iDs

E Trier https://orcid.org/0000-0002-6901-8669
M Willensdorfer https://orcid.org/0000-0002-1080-4200
S S Denk https://orcid.org/0000-0002-9077-4610
P Hennequin https://orcid.org/0000-0002-4848-4898
F Mink https://orcid.org/0000-0003-2995-2075
B Vanovac https://orcid.org/0000-0003-4031-9318

References

[1] Lopes Cardozo N J 1995 *Plasma Phys. Control. Fusion* **37** 799
[2] Ryter F, Dux R, Mantica P and Tala T 2010 *Plasma Phys. Control. Fusion* **52** 124043
[3] Garbet X *et al* 2004 *Plasma Phys. Control. Fusion* **46** 1351
[4] Suttrop W *et al* 1997 *Plasma Phys. Control. Fusion* **39** 2051
[5] Sauter O *et al* 2014 *Phys. Plasmas* **21** 055906
[6] Leonard A W, Groebner R J, Mahdavi M A, Osborne T H, Fenstermacher M E, Lasnier C J and Petrie T W 2002 *Plasma Phys. Control. Fusion* **44** 945
[7] Loarte A *et al* 2003 *Plasma Phys. Control. Fusion* **45** 1549
[8] Urano H, Suttrop W, Horton L D, Herrmann A and Fuchs J C 2003 *Plasma Phys. Control. Fusion* **45** 1571
[9] Callen J D and Jahns G L 1977 *Phys. Rev. Lett.* **38** 491
[10] Fredrickson E D, McGuire K, Cavallo A, Budny R, Janos A, Monticello D, Nagayama Y, Park W, Taylor G and Zarnstorff M C 1990 *Phys. Rev. Lett.* **65** 2869
[11] Fredrickson E D, Austin M E, Groebner R J, Manickam J, Rice B, Schmidt G and Snider R 2000 *Phys. Plasmas* **7** 5051
[12] Rathgeber S K, Barrera L, Eich T, Fischer R, Nold B, Suttrop W, Willensdorfer M, Wolfrum E and The ASDEX Upgrade Team 2013 *Plasma Phys. Control. Fusion* **55** 025004
[13] Willensdorfer M *et al* 2016 *Plasma Phys. Control. Fusion* **58** 114004
[14] Greenwald M J 2002 *Plasma Phys. Control. Fusion* **44** R27
[15] Snyder P, Wilson H, Ferron J, Lao L, Leonard A, Mossessian D, Murakami M, Osborne T, Turnbull A and Xu X 2004 *Nucl. Fusion* **44** 320
[16] Dunne M G, McCarthy P J, Wolfrum E, Fischer R, Giannone L, Burckhart A and The ASDEX Upgrade Team 2012 *Nucl. Fusion* **52** 123014
[17] Doyle E J *et al* 2007 *Nucl. Fusion* **47** S18
[18] Jacchia A, Mantica P, De Luca F and Gorini G 1991 *Phys. Fluids* B **3** 3033
[19] Ryter F *et al* 2001 *Plasma Phys. Control. Fusion* **43** 323
[20] Kirk A, Dunai D, Dunne M, Huijsmans G, Pamela S, Becoulet M, Harrison J R, Hillesheim J, Roach C and Saarelma S 2014 *Nucl. Fusion* **54** 114012
[21] Huysmans G T A and Czarny O 2007 *Nucl. Fusion* **47** 659
[22] Orain F *et al* 2013 *Phys. Plasmas* **20** 102510
[23] Hoelzl M *et al* 2018 *Contrib. Plasma Phys.* **58** 518
[24] Mink A F *et al* 2018 *Nucl. Fusion* **58** 026011
[25] Rechester A B and Rosenbluth M N 1978 *Phys. Rev. Lett.* **40** 38
[26] Lichtenberg A J, Itoh K, Itoh S I and Fukuyama A 1992 *Nucl. Fusion* **32** 495
[27] Yu Q 2006 *Phys. Plasmas* **13** 062310
[28] Meiss J D 1992 *Rev. Mod. Phys.* **64** 795
[29] Wobig H 1987 *Z. Naturforsch.* A **42** 1054
[30] Volpe F A, Kessler J, Ali H, Evans T E and Punjabi A 2012 *Nucl. Fusion* **52** 054017
[31] Hudson S R, Dewar R L, Dennis G, Hole M J, McGann M, von Nessi G and Lazerson S 2012 *Phys. Plasmas* **19** 112502
[32] Itoh K, Itoh S I, Fukuyama A, Tsuji S and Lichtenberg A J 1992 *Nucl. Fusion* **32** 1851
[33] Yu Q, Günter S and Finken K H 2009 *Phys. Plasmas* **16** 042301
[34] Ida K *et al* 2013 *New J. Phys.* **15** 013061
[35] Ida K, Kobayashi T, Yoshinuma M, Suzuki Y, Narushima Y, Evans T E, Ohdachi S, Tsuchiya H, Inagaki S and Itoh K 2016 *Nucl. Fusion* **56** 092001
[36] Schweinzer J *et al* 2016 *Nucl. Fusion* **56** 106007